energies

MDPI

Article

Design and Analysis of a Novel Opposite Trapezoidal Flow Channel for Solid Oxide Electrolysis Cell Stack

Zhen Zhang [1,2], Chengzhi Guan [1,3,4,*], Leidong Xie [5,*] and Jian-Qiang Wang [1,3,4,*]

[1] Department of Hydrogen Technique, Shanghai Institute of Applied Physics, Chinese Academy of Sciences, Shanghai 201800, China
[2] University of Chinese Academy of Sciences, Beijing 100049, China
[3] Key Laboratory of Interfacial Physics and Technology, Chinese Academy of Sciences, Shanghai 201800, China
[4] Dalian National Laboratory for Clean Energy, Dalian 116023, China
[5] Center for Thorium Molten Salts Reactor System, Shanghai Institute of Applied Physics, Chinese Academy of Sciences, Shanghai 201800, China
* Correspondence: guanchengzhi@sinap.ac.cn (C.G.); xieleidong@sinap.ac.cn (L.X.); wangjianqiang@sinap.ac.cn (J.-Q.W.)

Abstract: High efficiency, raw material availability, and compatibility with downstream systems will enable the Solid Oxide Electrolysis Cell (SOEC) to play an important role in the future energy transition. However, the SOEC stack's performance should be improved further by utilizing a novel flow-field design, and the channel shape is a key factor for enhancing gas transportation. To investigate the main effects of the novel channel design with fewer calculations, we assumed ideal gas laminar flows in the cathode channel. Furthermore, the cathode support layer thickness and electrical contact resistance are ignored. The conventional channel flow is validated first with mesh independence, and then the performance difference between the conventional and novel designs is analyzed using COMSOL Multiphysics. The process parameters such as velocity, pressure, current density, and mole concentration are compared between the conventional and novel designs, demonstrating that the novel design significantly improves electrolysis efficiency. Furthermore, it directly increased the concentration of product hydrogen in the novel channel. In addition to enhancing convection and diffusion of reaction gases in neighboring channels, the simple structure makes it easy to manufacture, which is advantageous for accelerating commercial use of the novel design.

Keywords: SOEC; stack; opposite trapezoidal; channel design; multiphysics; simulation

Citation: Zhang, Z.; Guan, C.; Xie, L.; Wang, J.-Q. Design and Analysis of a Novel Opposite Trapezoidal Flow Channel for Solid Oxide Electrolysis Cell Stack. *Energies* **2023**, *16*, 159. https://doi.org/10.3390/en16010159

Academic Editor: Erik Kjeang

Received: 16 November 2022
Revised: 9 December 2022
Accepted: 16 December 2022
Published: 23 December 2022

1. Introduction

Electrolysis technologies will play a critical role in the future energy transition [1]. It serves as a vital link between the electric, gas, and thermal grids, together with providing fuel for the transportation sector [2–5]. Compared with notable alkaline, polymer electrolyte membrane (PEM) technology, the solid oxide electrolysis cell (SOEC) has advantages such as higher conversion efficiencies and raw material availability [6]. Additionally, it can also integrate well with downstream chemical systems. SOECs are now fully prepared for industrial scale-up, and this scaling is already occurring at a rapid pace [7].

Although SOEC is a promising technology for the green energy transition, there are some issues that need to be resolved to accelerate its commercial application [8]. One of the most important problems is the gas distribution in the SOEC stack, which is relevant to the flow field in the interconnect [9]. Owing to the significant cell performance losses caused by poor gas transport, degradation, and low durability [10] may occur in the SOEC operating phase.

Many studies [11–16] have been conducted regarding the arrangement of channels in order to mitigate these negative effects caused by the flow field. In these channels, gas transport plays a paramount role in improving the performance of SOEC [17–19]. The

process of supplying reactant gases and wiping out the product gases is termed mass transport, which includes gas convection and gas diffusion. These two processes are determined by the shape of the channels. Therefore, channel design is absolutely the key factor for achieving SOEC performance enhancement. In recent years, most of the research [8,20–24] has focused on three different flow arrangements (co-flow, counter-flow, and cross-flow) of the straight channels to investigate their performance improvements. However, few studies [25] have involved how the channel shape impacts the mass transport in the stack.

In this study, a novel opposite trapezoidal channel with a simple design, handy fabrication, and specific capabilities for SOEC stack is elucidated. The main structure of a planar SOEC stack unit is shown in Figure 1. Key components of the SOEC stack, such as the interconnect, anode, electrolyte, and cathode, are depicted separately from top to bottom. In the traditional channel, high-temperature steam is fed into a porous cathode. When the steam diffuses to the three-phase boundary (TPB), it receives electrons from the current collector and then splits into hydrogen and oxygen ions. Afterward, the oxygen ions travel across the electrolyte to the anode, which is driven by the electric potential energy. Finally, the oxygen gas is generated and disperses into the air channel.

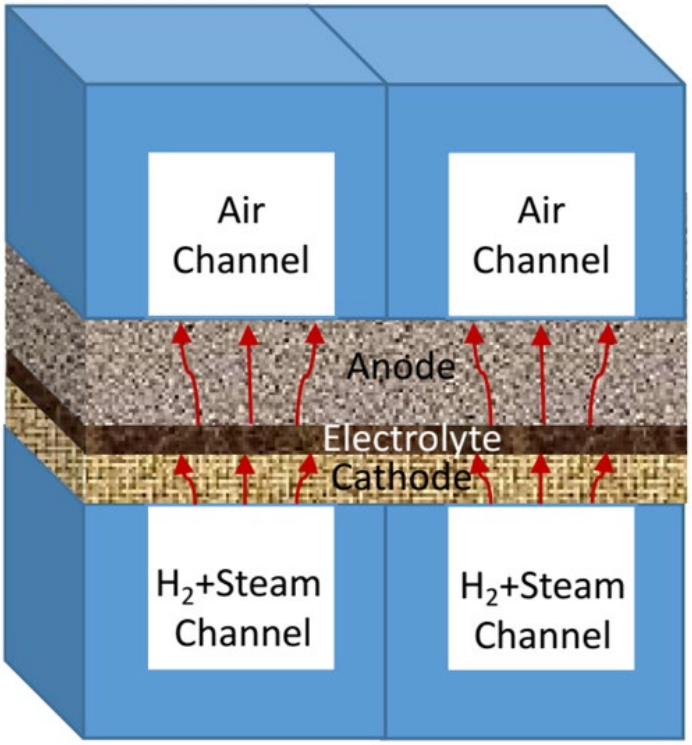

Figure 1. A typical planar SOEC stack-unit scheme.

Unlike the conventional SOEC channel design, the rib and channel width of the novel opposite trapezoidal design varies along the flow direction. The channels become wider in the middle of each section, and the ribs become narrower. This feature has the potential to produce uneven flow in order to enhance the direct exposure of reactants to the electrodes without affecting the cell's active area. More importantly, the novel design can increase reactant diffusion into the electrodes by changing the flow velocity and pressure along each channel. The potential benefits of the novel channels are investigated in terms of higher current densities and more efficient reactant distributions inside the SOEC. This novel design has more positive effects on the SOEC's performance and productivity.

2. SOEC Mathematical Model

To simplify the model and improve the calculating efficiency, the following assumptions are clarified in the following planar SOEC model:

- Sufficient and even oxidant distribution on the anode side;
- Laminar flow in the cathode channels;
- Ideal gas with no slip on the wall;
- Electrical contact resistance between the interconnect and the electrode is neglected;
- The thickness of the cathode support layer is omitted.

The SOEC mathematical model includes the following equations: mass conservation, momentum conservation, species conservation, and electrochemical equations.

2.1. Mass Conservation

Mass conservation is satisfied throughout the SOEC flow channels and porous electrodes [26]. The mass conservation equation can be described by the equation:

$$\nabla\cdot(\varepsilon\rho\boldsymbol{u}) = S_m \tag{1}$$

where ε denotes the porosity, ρ the density (kg m^{-3}), $\boldsymbol{u}$ the velocity (m s^{-1}), and S_m the mass source term.

2.2. Momentum Conservation

The flow of a mixture (steam and hydrogen) and air in the channel is laminar, which can be modeled using the following equation:

$$\varepsilon\rho(\boldsymbol{u}\cdot\nabla)\boldsymbol{u} = -\varepsilon\nabla p + \nabla\cdot\left(\mu\varepsilon\left(\nabla\boldsymbol{u} + (\nabla\boldsymbol{u})^T\right)\right) + S_u \tag{2}$$

where p is pressure (Pa), μ the dynamic viscosity (Pa s), and S_u the source item (N m^{-3}); in-channel, $S_u = 0$ and in-electrode, $S_u = -\mu/Bu$.

The Brinkman equation is applied to compute single-phase fluid velocity and pressure fields in porous media in the laminar flow regime [27]:

$$\left(\frac{\mu}{k} + S_m\right)\boldsymbol{u} = \nabla\cdot\left[-pI + \frac{\mu}{\varepsilon}\left(\nabla\boldsymbol{u} + (\nabla\boldsymbol{u})^T - \frac{2}{3}(\nabla\boldsymbol{u})I\right)\right] \tag{3}$$

where k denotes permeability of the electrode, S_m is the mass source term, and I is the unit vector.

2.3. Species Conservation

The species transfer equation can be expressed as:

$$\begin{array}{l}\nabla\cdot(\varepsilon\rho\boldsymbol{u}Y_i) = \nabla\cdot(\rho D_i\nabla(Y_i)) + S_i \\ S_i:\ S_{H_2} = M_{H_2}\, j/(2F),\ S_{H_2O} = M_{H_2O}\, j/(2F),\ S_{O_2} = M_{O_2}\, j/(4F).\end{array} \tag{4}$$

where Y_i and D_i are the mass fraction and effective diffusion coefficient (m^2 s^{-1}) of species i, respectively; M_i is the mole weight of species i, j current density (A m^{-2}), F is Faraday's constant.

2.4. Electrochemical Equations

The process of high-temperature water electrolyzing can be expressed by the following two electrochemical equations:

$$H_2O + 2e^- \rightarrow\ H_2 + O^{2-} \tag{5}$$

$$O^{2-} - 4e^- \rightarrow\ O_2 \tag{6}$$

Charge balance and the theoretical voltage equations can refer to [8].

2.5. Geometries and Boundary Conditions

The sizes and geometries of the two different channels are shown in Figure 2. For instance, it is assumed that the gas feeds into the inlet on the right-downside, then comes into the contracted section at the throat of the channel, and finally runs into the expanded section of the channel for a repeated unit.

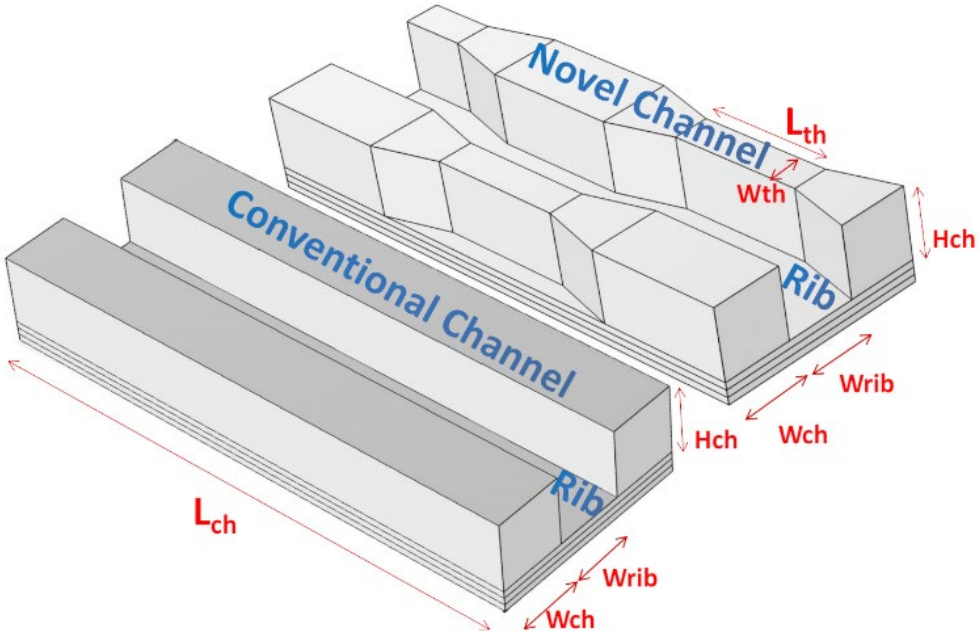

Figure 2. A geometry comparison between the conventional channel and the novel channel.

For the geometric and operating parameter comparison between the conventional channel and the novel channel, see Table 1.

Table 1. Geometric and operating parameters for the SOEC with the conventional and the novel channel.

SOEC Parameter	Conventional Channel	Novel Channel	Unit
Channel length (L_{ch})	8	8	mm
Channel width (W_{ch})	1	1	mm
Channel height (H_{ch})	1	1	mm
Rib width (W_{rib})	1	-	mm
Throat width (W_{th})	-	0.5	mm
Throat length (L_{th})	-	2	mm
Anode thickness	20	20	um
Electrolyte thickness	20	20	um
Cathode thickness	20	20	um
Cathode support layer thickness	280	280	um
Cathode porosity	0.5	0.5	-
Cathode permeability	1.00×10^{-12}	1.00×10^{-12}	m^2
Electrolyte conductivity	5	5	S/m
Cathode conductivity	1000	1000	S/m

On the wall of the channel, no-slip boundary conditions are applied. At the inlet of the channel, a constant mass flow rate and species flux are maintained. The details of boundary conditions are shown in Table 2.

Table 2. Boundary conditions of the conventional channel and the novel channel.

SOEC Parameter	Conventional Channel	Novel Channel	Unit
Inlet velocity	0.1	0.1	m/s
Outlet pressure	0	0	Pa
Hydrogen mole fraction at the cathode inlet	0.1	0.1	-
Steam mole fraction at the cathode inlet	0.9	0.9	-
Boundary electric potential value	1	1	V

3. Model Implementation and Validation

Physical laws for space- and time-dependent problems are typically expressed in terms of partial differential equations (PDEs), and the accounting parts in this article are the governing equations listed in the previous section. These equations cannot be solved analytically for the vast majority of geometries and problems. Instead, an approximation of the equations can be built, typically using various types of discretization. These discretization techniques approximate the PDEs with numerical model equations that can be solved numerically. The numerical model equation solutions are, in turn, an approximation of the real PDE solutions. Such approximations are commonly called the finite element method (FEM).

Unlike the PDE form of governing equations described previously, they are transformed into the weak form and then numerically solved in COMSOL Multiphysics built-in modules. Before that, the weak-form equations are discretized into different shapes of meshes. The simulations are run for various grid sizes and types to ensure that the results are independent of grid size and type [28].

The FEM discretization meshes of the conventional channel and the novel channel are shown in Figure 3a. The element type includes tetrahedra, pyramids, prisms, triangles, quads, edge, and vertex elements. An optimal mesh is required for simulation due to the time/space efficiency and calculation accuracy. The mesh independence validation of gas velocity in channels are shown in Figure 3b,c. The total number of elements in the conventional channel is 303,388, while the elements number in the novel channel is 431,956. There are approximately 11,881,328 degrees of freedom in the computational domain. The solutions converge after 3500 iterations. A convergence criterion of 10^{-4} is used for all variables.

Since the opposite trapezoidal flow channel is a new design concept, the corresponding experimental data are not available. In fact, there are few studies involved in the simulation of the SOEC channel flow field. Navasa [29] built a three-dimensional CFD model for performance evaluation of a solid oxide electrolysis cell for hydrogen production. Ni [30,31] simulated the fluid dynamic and chemical reactions of SOEC for hydrogen production. Cacciuttolo [32] verified the effect of pressure on SOEC by COMSOL Multiphysics. As commercial software, the capability maturity model for COMSOL Multiphysics is verified by all kinds of users.

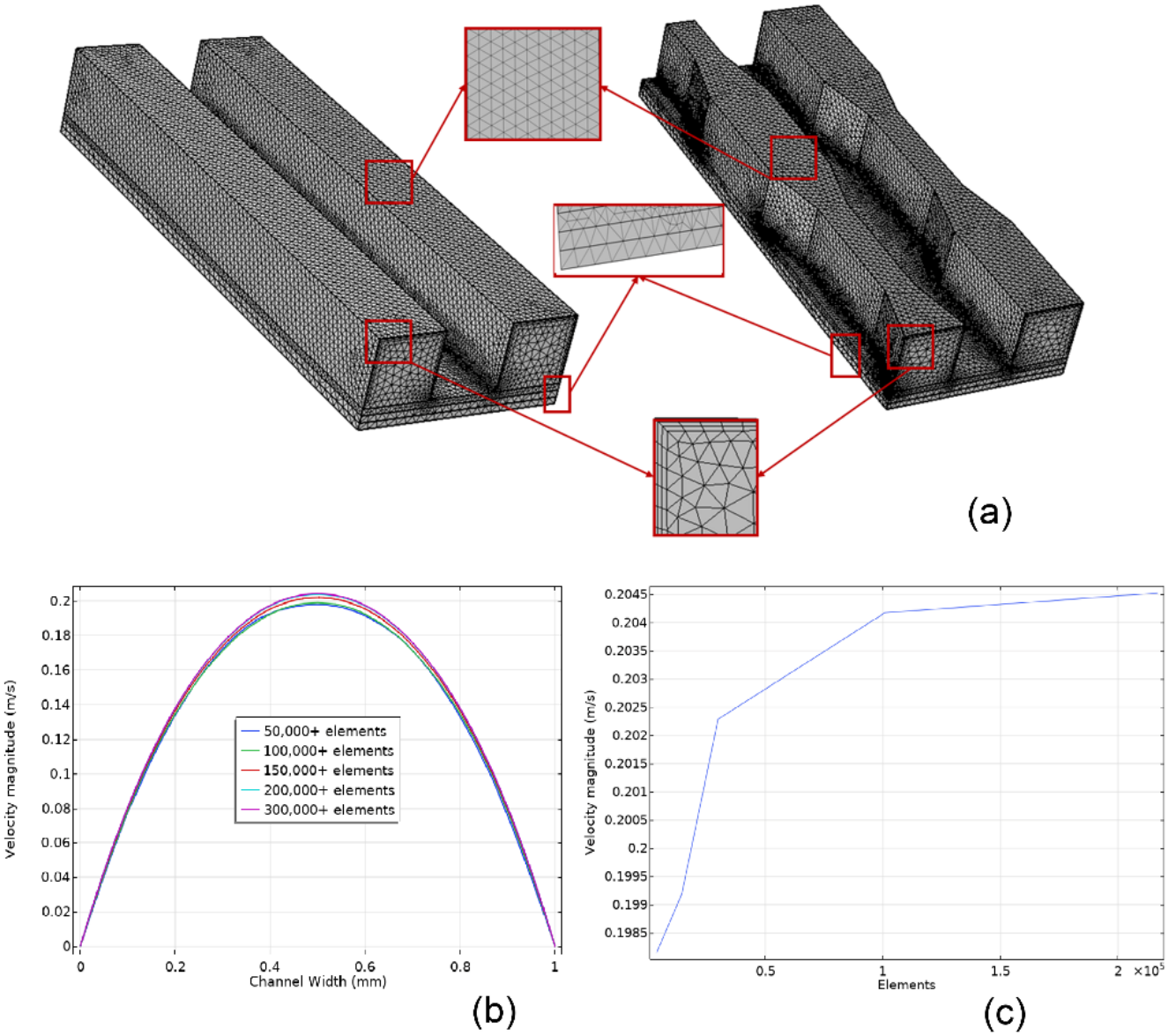

Figure 3. Mesh independence validation: (**a**) FEM discretization mesh of the conventional channel and the novel channel; (**b**) channel gas velocity magnitude lines with a variety of elements; (**c**) channel gas velocity probe curve with different elements.

4. Results and Discussion

The continuous straight channel structure is commonly used in the SOEC stack. However, due to the rib coverage, it is difficult to convey reaction gas to the electrode region beneath the ribs in a timely manner via gas diffusion, which degrades the local cell performance beneath the ribs and thus reduces the whole stack's performance.

To address the issue, we propose a novel channel design that can efficiently improve gas diffusion. The current densities are obtained and compared based on the output voltage to elaborate on the change in output performance of SOEC with different channels.

4.1. Channel Velocity Distribution

Figure 4 shows the difference in mixed gas velocity distribution between the conventional design and the novel design on the cathode side. It is found that the velocity decreases from 0.25 m/s in the central region to 1.70×10^{-5} m/s in the vicinity of the wall in the conventional channels. Owing to the isobars being at the same coordinate point between the neighboring conventional channels, the velocity distribution is synchronic

along the flow direction. However, in the novel channels, the velocity changes sharply according to the channel geometry along the flow direction.

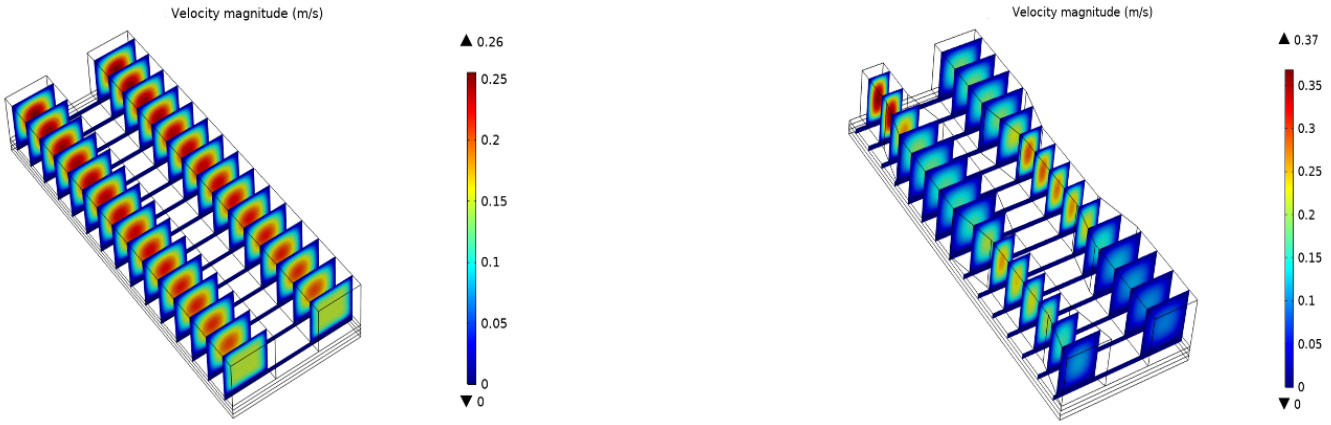

Figure 4. Velocity distribution in conventional channel and novel channel.

It is uniformly distributed in the straight part at an average velocity of 0.10 m/s increases to 0.30 m/s in the contraction section, then slows to 0.15 m/s in the expansion section, and this phenomenon is consistent with the Bernoulli equation [33]. The asynchronic velocity change in the neighboring novel channels generates the pressure gradient at the same coordinate point along the flow direction.

4.2. Channel Pressure Profile

From the discussions in the previous section, it is noted that in the novel channels, the velocity changes according to the geometry, which represents the pressure variation shown in Figure 5. From the left side of the figure, it is clear that there is no pressure change in the perpendicular direction of channels between the neighboring conventional channels. The total pressure loss from inlet to outlet in the conventional channel is about 0.26 Pa.

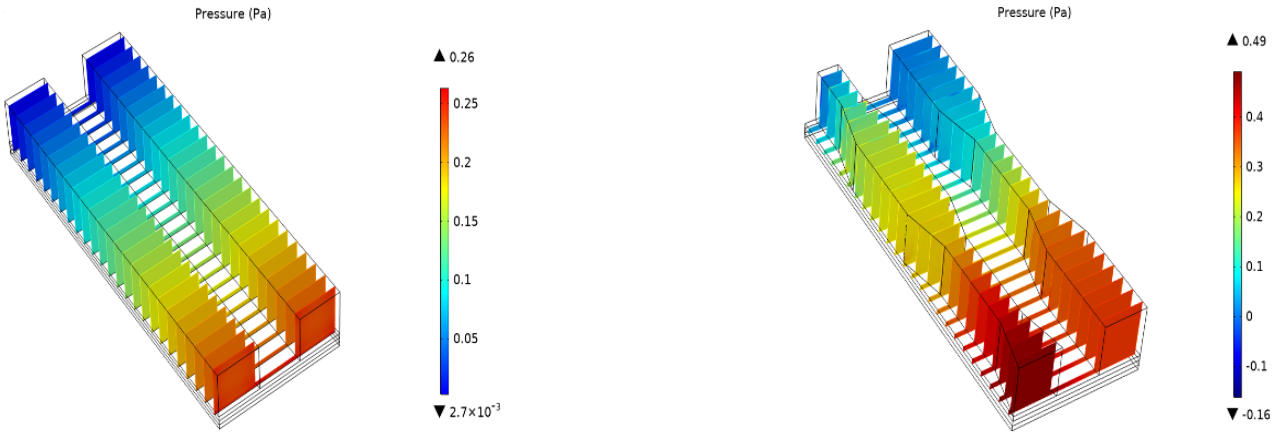

Figure 5. Pressure profile in conventional channel and novel channel.

From the right side of Figure 4, it is found that the pressure changes along the flow direction in the novel channels. In the meantime, the value of the pressure gradient is about 0.10 Pa in the perpendicular direction of channels, which improves the gas convection in the neighboring novel channels. Furthermore, it accelerates the electrical reaction in the appropriate place compared to the conventional design. On the one hand, the pressure gradient is beneficial for gas exchange. On the other hand, from the figuration, it shows that the pressure drop from inlet to outlet is as large as 0.40 Pa. The total pressure loss in the novel design is greater than it is in the conventional design.

4.3. Current Density

Figure 6 depicts the current density distribution on the reaction surface of different designs. From the figure on the left side, it shows that the average current density is lower than its counterpart on the right side. In most parts of the electrolyte, the current density is 0.40 $\times$ 10^3 A/m^2 on the conventional channel side. However, the current density is more than 1.00 $\times$ 10^3 A/m^2 on the novel channel side except for the expanded regions. Particularly, regions under the ribs have a high current density, which can be attributed to the increased gas flux between neighboring channels discussed in the previous section.

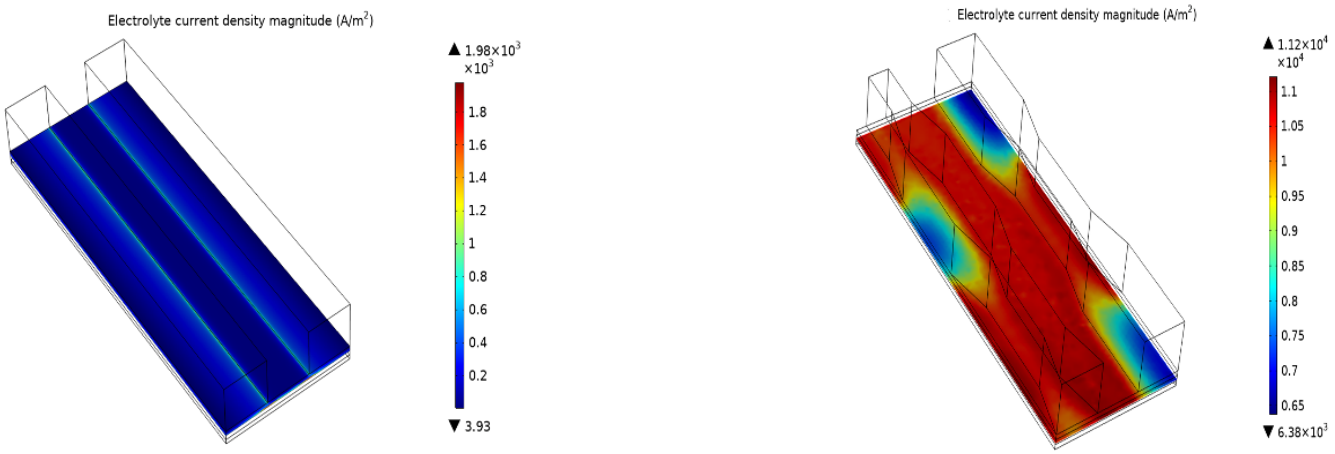

Figure 6. Current density distribution in the conventional channel and the novel channel.

The gas flow rate slows in the expanded area of the novel channel, so the pressure increases accordingly, which makes the gas in these regions more likely to diffuse to other low-pressure regions. It will eventually result in a reaction gas deficit, or a lower current density.

4.4. Water Vapor Mole Fraction Distribution

Figure 7 presents the water vapor mole fraction in the channels of different designs. It demonstrates that the concentration of water vapor in the cathode electrode (15.0 mol/m^3) in the conventional channels is lower than that (30.0 mol/m^3) in the novel channel. Significant concentration gradients of the water vapor mole fraction are observed at the inlet and outlet of the novel channels. Water vapor diffusion and thus consumption are generally mildly along the flow direction. Clearly, the gas swing between the neighboring channels enhances the water vapor consumption. As a result, the vapor concentration decreases sharply from 40.0 mol/m^3 to around 20.0 mol/m^3 along the channel.

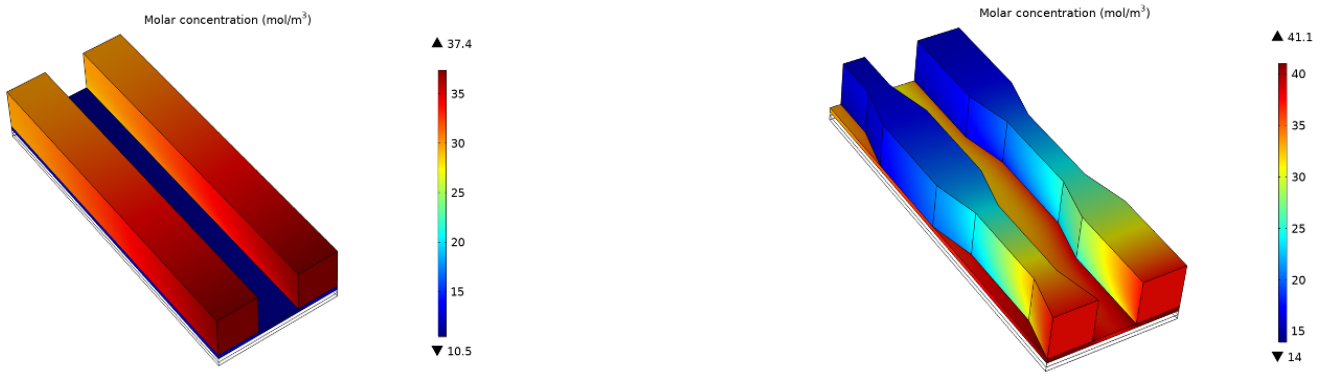

Figure 7. Water vapor mole fraction distribution in conventional channel and novel channel.

In contrast, the concentration of water vapor in the conventional channels changes relatively little and decreases from 37.0 mol/m^3 to 30.0 mol/m^3 accordingly.

4.5. Hydrogen Mole Fraction Distribution

The greater the diffusion of reactant gases into the electrodes, the more reactions occur over the TPB in the electrode. Figure 8 depicts the mole concentration variation in product hydrogen. As illustrated on the left side of the figure, the mole concentration of hydrogen increased from 4.0 mol/m^3 in the inlet to 11.0 mol/m^3 in the outlet. At the same time, the mole concentration of hydrogen is below 2.0 mol/m^3 under the rib.

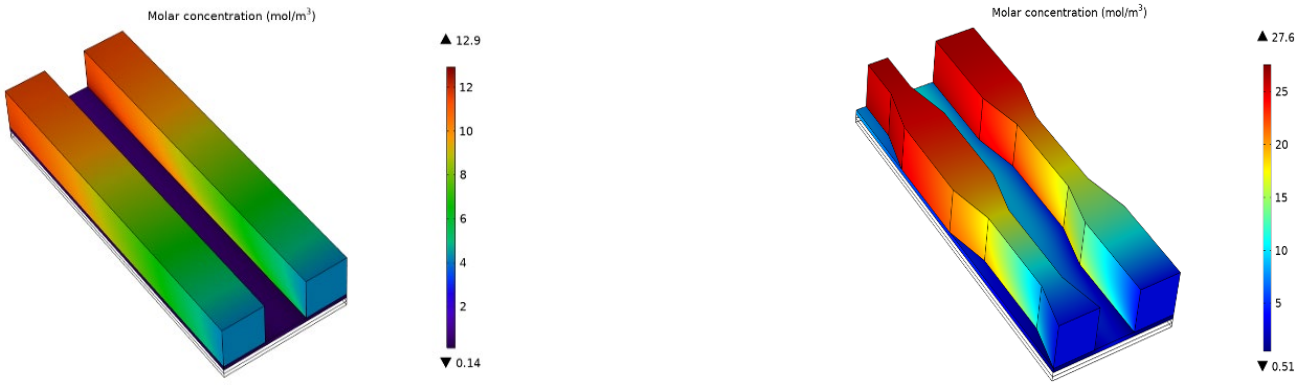

Figure 8. Hydrogen mole fraction distribution in conventional channel and novel channel.

On the contrary, in the novel channels, the mole concentration of hydrogen increases from 5.0 mol/m^3 at the inlet to 25.0 mol/m^3 at the outlet, and the hydrogen concentration under the rib is around 10.0 mol/m^3.

It is worth noting that the hydrogen concentration (5.0 mol/m^3) in the electrode of the novel channel is twice as high as that in the conventional channel (2.5 mol/m^3). The cell performance or provision of high hydrogen concentration, as is the case with the optimized channel geometry for commercial purposes, is the most important criterion for selecting the proper SOEC design. For designs with novel opposite trapezoidal channels, it is nearly 2.7 times more efficient, providing a high number of reactants in the electrode and resulting in more hydrogen production by the same electrolysis process.

5. Conclusions

An exhaustive numerical investigation was conducted to compare the electrolysis performance between the conventional channel design and the novel opposite trapezoidal channel design. The current density of the novel design (1.0×10^3 A/m^2) is found to be much higher than its counterpart (0.4×10^3 A/m^2) in the conventional design. Moreover, the water vapor concentration of the electrode in the novel channel is twice as high as it is in the conventional channel, which leads to the product hydrogen concentration (25.0 mol/m^3) in the outlet of the novel channel, increasing sharply compared to the conventional channel (10.0 mol/m^3). From the study of the two different channels, the novel channel has several significant advantages over the conventional one:

- Significantly higher water vapor diffusivity into the cathode electrode;
- Remarkably higher current and electrolysis efficiency per unit active area;
- Improved the mass transfer between the neighboring channels and the distribution of reactants being noticeably more uniform;
- The novel channels are tractable and economical in the manufacturing process.

Author Contributions: Conceptualization, C.G.; validation, Z.Z.; formal analysis, Z.Z.; investigation, Z.Z.; resources, L.X. and J.-Q.W.; data curation, Z.Z.; writing—original draft, Z.Z.; supervision, C.G., L.X., and J.-Q.W.; project administration, L.X. and J.-Q.W.; funding acquisition, L.X. and J.-Q.W. All authors have read and agreed to the published version of the manuscript.

Funding: This research was funded by the Transformational Technologies for Clean Energy and Demonstration Strategic Priority Research Program of the Chinese Academy of Sciences (No. XDA2100000), the Youth Innovation Promotion of the Chinese Academy of Sciences (No. 2021253), and the Ministry of Science and Technology of China (No. 2021YFE0100200), Pakistan Science Foundation (PSF) Project (No. PSF/CRP/18thProtocol (01)).

Institutional Review Board Statement: Not applicable.

Informed Consent Statement: Not applicable.

Data Availability Statement: Not applicable.

Conflicts of Interest: The authors declare no conflict of interest.

Nomenclature

Effective diffusion coefficient ($m^2\ s^{-1}$)	D_i
Faraday constant, 96,485 ($C\ mol^{-1}$)	F
Channel height (mm)	H_{ch}
Unit vector	I
Electrical current density ($A\ m^{-2}$)	J
Permeability of the electrode ($S\ m^{-1}$)	k
Channel length (mm)	L_{ch}
Throat length (mm)	L_{th}
Environment pressure (Pa)	p
Mole weight of species i	M_i
Gas velocity ($m\ s^{-1}$)	U
Channel width (mm)	W_{ch}
Rib width (mm)	W_{rib}
Throat width (mm)	W_{th}
Mass fraction	Y_i
Greek symbols	
Gas density ($kg\ m^{-3}$)	ρ
Viscosity ($kg\ m^{-1}\ s^{-1}$)	μ
Electrode porosity	ξ
Subscript	
Channel	Ch
Rib	rib
Throat	Th

References

1. Wappler, M.; Unguder, D.; Lu, X.; Ohlmeyer, H.; Teschke, H.; Lueke, W. Building the green hydrogen market–Current state and outlook on green hydrogen demand and electrolyzer manufacturing. *Int. J. Hydrog. Energy* **2022**, *47*, 20. [CrossRef]
2. Hauch, A.; Kungas, R.; Blennow, P.; Hansen, A.B.; Hansen, J.B.; Mathiesen, B.V.; Mogensen, M.B. Recent advances in solid oxide cell technology for electrolysis. *Science* **2020**, *370*, 10. [CrossRef] [PubMed]
3. Capurso, T.; Stefanizzi, M.; Torresi, M.; Camporeale, S.M. Perspective of the role of hydrogen in the 21st century energy transition. *Energy Convers. Manag.* **2022**, *251*, 17. [CrossRef]
4. Maestre, V.M.; Ortiz, A.; Ortiz, I. Challenges and prospects of renewable hydrogen-based strategies for full decarbonization of stationary power applications. *Renew. Sustain. Energy Rev.* **2021**, *152*, 24. [CrossRef]
5. Wanbing Guan, G.W.; Xiao-Dong, Z. Mechanism of the cathode current collector on cell performance in a solid oxide fuel cell stack. *J. Power Sources* **2017**, *351*, 5.
6. Lebrouhi, B.E.; Djoupo, J.J.; Lamrani, B.; Benabdelaziz, K.; Kousksou, T. Global hydrogen development–A technological and geopolitical overview. *Int. J. Hydrog. Energy* **2022**, *47*, 33. [CrossRef]
7. Zamudio-García, J.; Caizán-Juanarena, L.; Porras-Vázquez, J.M.; Losilla, E.R.; Marrero-López, D. A review on recent advances and trends in symmetrical electrodes for solid oxide cells. *J. Power Sources* **2022**, *520*, 27. [CrossRef]

8. Yang, C.; Guo, R.; Jing, X.; Li, P.; Yuan, J.; Wu, Y. Degradation mechanism and modeling study on reversible solid oxide cell in dual-mode—A review. *Int. J. Hydrog. Energy* **2022**, *47*, 34. [CrossRef]
9. Heenan, T.M.; Nabavi, S.A.; Erans, M.; Robinson, J.B.; Kok, M.D.; Maier, M.; Daniel, J.L.B.; Paul, R.S.; Vasilije, M. The Role of Bi-Polar Plate Design and the Start-Up Protocol in the Spatiotemporal Dynamics during Solid Oxide Fuel Cell Anode Reduction. *Energies* **2020**, *13*, 12. [CrossRef]
10. Zhen Zhang, Y.Y.; Guan, C.; Cheng, F.; Xie, J.; Lu, Y.; Wang, J.Q. Numerical study on the inhomogeneity of the contact layer between solid oxide electrolysis cell. *Fuel Cells* **2022**, *1*, 7. [CrossRef]
11. Heidary, H.; Abbassi, A.; Kermani, M.J. Enhanced heat transfer with corrugated flow channel in anode side of direct methanol fuel cells. *Energy Convers. Manag.* **2013**, *75*, 13. [CrossRef]
12. Atul Kumar, R.G.R. Effect of channel dimensions and shape in the flow-field distributor on the performance of polymer electrolyte membrane fuel cells. *J. Power Sources* **2003**, *113*, 8.
13. Chen, B.; Xu, H.; Ni, M. Modelling of finger-like channelled anode support for SOFCs application. *Sci. Bull.* **2016**, *61*, 9. [CrossRef]
14. Dong, D.; Shao, X.; Hu, X.; Chen, K.; Xie, K.; Yu, L.; Ye, Z.; Yang, P.; Parkinson, G.; Li, C.-Z. Improved gas diffusion within microchanneled cathode supports of SOECs for steam electrolysis. *Int. J. Hydrog. Energy* **2016**, *41*, 7. [CrossRef]
15. Huang, C.M.; Shy, S.S.; Lee, C.H. On flow uniformity in various interconnects and its influence to cell performance of planar SOFC. *J. Power Sources* **2008**, *183*, 9. [CrossRef]
16. Zhonggang Zhang, J.C.; Yue, D.; Yang, G.; Ye, S.; He, C.; Wang, W.; Yuan, J.; Huang, N. Three-Dimensional CFD Modeling of Transport Phenomena in a Cross-Flow Anode-Supported Planar SOFC. *Energies* **2014**, *7*, 19. [CrossRef]
17. Duhn, J.D.J. Anker Degn; Wedel, Stig; Wix, Christian Optimization of a new flow design for solid oxide cells using computational fluid dynamics modelling. *J. Power Sources* **2016**, *336*, 11. [CrossRef]
18. Dash, A.P.; Alam, T.; Siddiqui, M.I.H.; Blecich, P.; Kumar, M.; Gupta, N.K.; Masood, A.; Yadav, A.S. Impact on Heat Transfer Rate Due to an Extended Surface on the Passage of Microchannel Using Cylindrical Ribs with Varying Sector Angle. *Energies* **2022**, *15*, 24. [CrossRef]
19. Liu, H.; Akhtar, Z.; Li, P.; Wang, K. Mathematical Modeling Analysis and Optimization of Key Design Parameters of Proton-Conductive Solid Oxide Fuel Cells. *Energies* **2014**, *7*, 18. [CrossRef]
20. Su, S.; He, H.; Chen, D.; Zhu, W.; Wu, Y.; Kong, W.; Wang, B.; Lu, L. Flow distribution analyzing for the solid oxide fuel cell short stacks with rectangular and discrete cylindrical rib configurations. *Int. J. Hydrog. Energy* **2015**, *40*, 16. [CrossRef]
21. Schluckner, C.; Subotić, V.; Preißl, S.; Hochenauer, C. Numerical analysis of flow configurations and electrical contact positions in SOFC single cells and their impact on local effects. *Int. J. Hydrog. Energy* **2019**, *44*, 19. [CrossRef]
22. Wang, J. Theory and practice of flow field designs for fuel cell scaling-up: A critical review. *Appl. Energy* **2015**, *157*, 24. [CrossRef]
23. Wei, S.S.; Wang, T.H.; Wu, J.S. Numerical modeling of interconnect flow channel design and thermal stress analysis of a planar anode-supported solid oxide fuel cell stack. *Energy* **2014**, *69*, 9. [CrossRef]
24. Zhang, Z.; Yue, D.; Yang, G.; Chen, J.; Zheng, Y.; Miao, H.; Wang, W.; Yuan, J.; Huang, N. Three-dimensional CFD modeling of transport phenomena in multi-channel anode-supported planar SOFCs. *Int. J. Heat Mass Transf.* **2015**, *84*, 13. [CrossRef]
25. Khazaee, I.; Rava, A.R. Numerical simulation of the performance of solid oxide fuel cell with different flow channel geometries. *Energy* **2017**, *119*, 10. [CrossRef]
26. Jin, X.; Xue, X. Mathematical modeling analysis of regenerative solid oxide fuel cells in switching mode conditions. *J. Power Sources* **2010**, *195*, 7. [CrossRef]
27. Shi, J.; Xue, X. CFD analysis of a novel symmetrical planar SOFC design with micro-flow channels. *Chem. Eng. J.* **2010**, *163*, 7. [CrossRef]
28. Shah, I.; Kim, S.W.; Kim, K.; Doh, Y.H.; Choi, K.H. Experimental and numerical analysis of Y-shaped split and recombination micro-mixer with different mixing units. *Chem. Eng. J.* **2019**, *358*, 16. [CrossRef]
29. Navasa, M.; Yuan, J.; Sundén, B. Computational fluid dynamics approach for performance evaluation of a solid oxide electrolysis cell for hydrogen production. *Appl. Energy* **2015**, *137*, 10. [CrossRef]
30. Ni, M.; Leung, M.K.H.; Leung, D.Y.C. Mathematical modeling of the coupled transport and electrochemical reactions in solid oxide steam electrolyzer for hydrogen production. *Electrochem. Acta* **2007**, *52*, 12. [CrossRef]
31. Ni, M. Computational fluid dynamics modeling of a solid oxide electrolyzer cell for hydrogen production. *Int. J. Hydrog. Energy* **2009**, *34*, 12. [CrossRef]
32. Cacciuttolo, Q.; Vulliet, J.; Lair, V.; Cassir, M.; Ringuedé, A. Effect of pressure on high temperature steam electrolysis: Model and experimental tests. *Int. J. Hydrog. Energy* **2015**, *40*, 7. [CrossRef]
33. Chanson, H. *Hydraulics of Open Channel Flow: An Introduction Basic Principles, Sediment Motion, Hydraulic Modelling, Design of Hydraulic Structures, 2 ed.*; Elsevier: Amsterdam, The Netherlands, 2004; p. 26.